Detection of windthrows and insect outbreaks by L-band SAR: A case study in the Bavarian Forest National Park

Mihai A Tanase, Cristina Aponte, Stéphane Mermoz, Alexandre Bouvet, Thuy Le Toan, Marco Heurich

Remote Sensing of Environment 209 (2018) 700–711

Contents lists available at ScienceDirect

Remote Sensing of Environment

journal homepage: www.elsevier.com/locate/rse

Detection of windthrows and insect outbreaks by L-band SAR: A case study in the Bavarian Forest National Park

Mihai A. Tanase[a,b,*], Cristina Aponte[b], Stéphane Mermoz[c], Alexandre Bouvet[c], Thuy Le Toan[c], Marco Heurich[d,e]

[a] Department of Geology, Geography and Environment, University of Alcala, C. Colegios 2, Alcala de Henares 28801, Spain
[b] School of Ecosystem and Forest Sciences, University of Melbourne, Parkville 3052, Australia
[c] Center for the Study of the Biosphere from Space, University of Paul Sabatier, 18 av. Edouard Belin, Toulouse 2801, France
[d] Department of Conservation and Research, Bavarian Forest National Park, Freyunger Straße 2, 94481 Grafenau, Germany
[e] Chair of Wildlife Ecology and Wildlife Management, University of Freiburg, Tennenbacher Straße 4, 79106 Freiburg, Germany

ARTICLE INFO

Keywords:
Insect outbreaks
Windthrows
Bark beetle
L-band SAR
ALOS PALSAR
Forest disturbance
Change detection
Radar change ratio

ABSTRACT

Natural disturbances significantly influence forest ecosystem services and biodiversity. Accurate delineation and early detection of areas affected by wind and insect outbreaks are crucial for guiding management decisions. To this end, past studies relied mostly on passive sensors (e.g., optical), and active sensors (i.e., radar) were rarely used. This study used L-band space-borne synthetic aperture radar (SAR) within a change-detection framework to delineate forested areas affected by wind and insect disturbances. The results showed that changes in backscatter relate to damage caused by wind and insect outbreaks. Overall accuracies of 69–84% and 65–88% were obtained for delineation of areas affected by wind damage and insect outbreaks, respectively, depending on the acquisition date and environmental conditions. Areas susceptible to insect outbreaks or experiencing the initial outbreak phase (green) were detected with lower accuracies (64–74%). It is expected that L-band space-borne SAR data can be applied over larger areas and ecosystem types in the temperate and boreal regions to delineate and detect damaged areas.

1. Introduction

Disturbances caused by windthrows or insect outbreaks play an immanent role in the dynamics of most forest ecosystems (Franklin et al., 2002; Turner et al., 1998). Worldwide, about 14 million hectares of forest are affected annually by abiotic agents other than fire, including 8.5 million hectares affected by insects, 3.8 million hectares affected by severe weather, and 1.2 million hectares affected by various diseases (Lierop et al., 2015). In temperate forests, insect outbreaks and severe weather conditions can affect 50 times as much forest area as fires (Dale et al., 2001).

Windthrows and insect outbreaks are influenced by global change in several ways (Schlyter et al., 2006). For example, extreme climate events in combination with a higher mean temperature decrease forest vitality, which in turn increases forest susceptibility to windthrows. Windthrows, in turn, often trigger insect outbreaks, which are then facilitated by warm and dry weather conditions (Seidl et al., 2016). In recent years, disturbance events reached an unprecedented global extent (Weed et al., 2013). Future climate projections predict that disturbances will further intensify (Seidl et al., 2014; Westerling et al., 2006), with potentially major impacts on global carbon sequestration (Kurz et al., 2008). Therefore, accurate monitoring of disturbance type, size, and impact over large areas is becoming increasingly important. In addition, early detection could support timely salvage logging operations and thereby minimize economic losses (Fahse and Heurich, 2011), or could allow short-term actions aimed at reducing the ecological impact of disturbance.

The European spruce bark beetle (*Ips typographus*) is the most important biotic disturbance agent in Europe and Siberia; other bark beetle species (e.g., *Dendroctonus ponderosae*, *Dendroctonus frontalis*) constitute major disturbance agents of coniferous forests in North America. Ignited by windthrows and droughts, bark beetle populations can reach very high densities, which allow them to kill even healthy trees (Marini et al., 2017). After hibernation, *I. typographus* beetles start to swarm in spring and lay their eggs underneath the inner bark of Norway spruce trees (*Picea abies*). Once the larvae hatch, they feed on the tree's phloem tissues, thus interrupting the flow of water and nutrients, which causes the tree to die. Infested trees go through three

* Corresponding author at: Department of Geology, Geography and Environment, University of Alcala, C. Colegios 2, Alcala de Henares 28801, Spain.
E-mail address: mihai@tma.ro (M.A. Tanase).

https://doi.org/10.1016/j.rse.2018.03.009
Received 22 April 2017; Received in revised form 21 February 2018; Accepted 5 March 2018

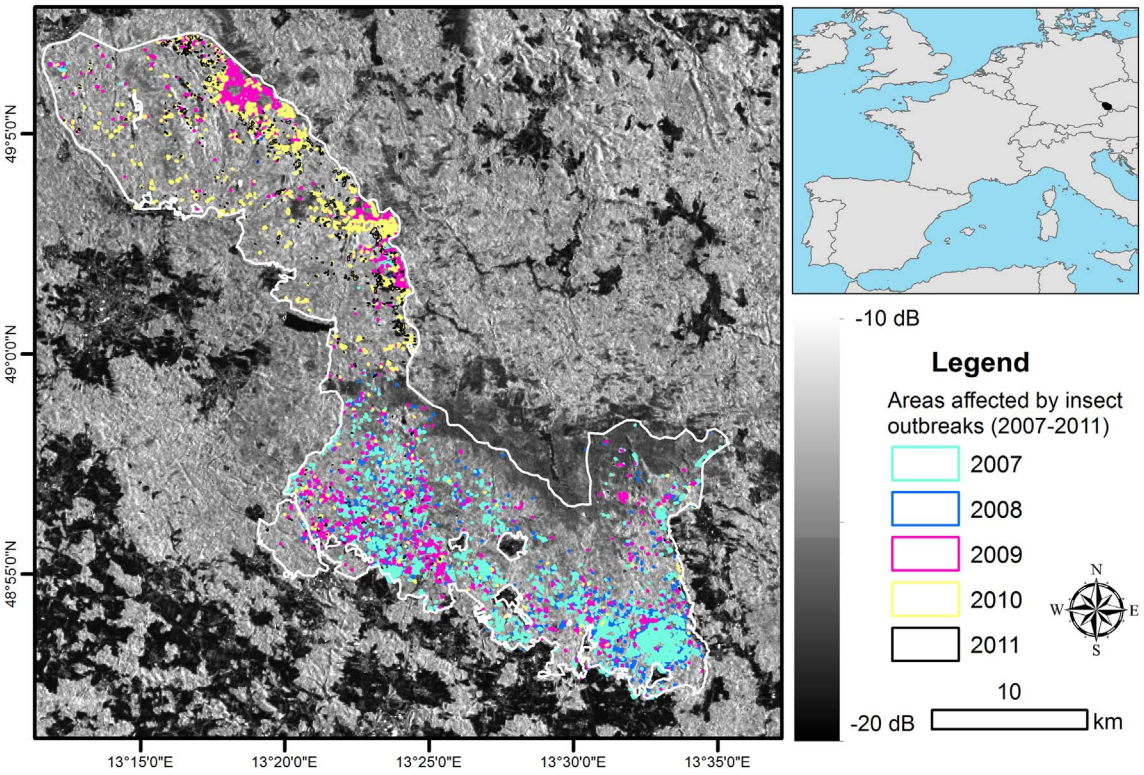

Fig. 1. Location of the Bavarian Forest National Park (white polygon) and the areas affected by insect outbreaks between 2007 and 2010 derived by aerial imagery interpretation. The background is represented by HV-polarized ALOS backscatter acquired on August 11, 2007.

stages of infestation named after the appearance of the trees, namely green, red, and gray attack stages, which are reached after a few days, a few months, and about half a year, respectively. In a forest, this process can occur up to three times a year (depending on temperature) because the beetle population can produce several generations per summer season (Wermelinger, 2004b).

Multiple within-year events can be separated only by frequent monitoring during spring and summer. Such monitoring can be cost effective over large areas only if remote-sensing technologies are used. Indeed, over the past decades, forest disturbance has received considerable attention by researchers that use remote sensing. Passive sensors of various spatial and spectral resolution have been employed for mapping insect-related disturbances (Frolking et al., 2009; Senf et al., 2017; Wulder et al., 2006), with methods spanning from the detection of single dead trees with very high-resolution aerial photography (Nielsen et al., 2014; Polewski et al., 2015), to taking advantage of multi-temporal algorithms based on the extensive Landsat time series archive (Cohen et al., 2010; Huang et al., 2010; Kennedy et al., 2010; Oeser et al., 2017), and to the use of hyperspectral sensors for the detection of the green attack stage (Fassnacht et al., 2014; Lausch et al., 2013).

The lack of long synthetic aperture radar (SAR) time series acquired from sensors with similar or compatible specifications has hindered the development of multi-temporal algorithms using active radar sensors. SAR-derived forest disturbance has largely been based on two-date change-detection techniques (Joshi et al., 2015; Kuntz and Siegert, 1999; Mitchard et al., 2011; Rignot and Zyl, 1993; Tanase et al., 2015a). Such studies, mostly focused on fire and logging induced disturbances, show that the L-band is one of the most sensitive SAR wavelengths for detecting disturbance effects in forested landscapes and that its sensitivity does not change across environments (Mermoz and Le Toan, 2016; Tanase et al., 2015b). In contrast, wind induced disturbance has been less considered, with only few SAR based studies being available (Eriksson et al., 2012; Fransson et al., 2010; Fransson et al., 2002; Green, 1998; Schwarz et al., 2003). Furthermore, a recent literature review on the remote sensing of insect disturbances almost exclusively mentions passive optical sensors (Senf et al., 2017), except for one study that combined active and passive technologies (Ortiz et al., 2013).

None of the active-based studies have taken advantage of the improved capabilities demonstrated by recent L-band space-borne platforms for delineating areas affected by insect outbreaks. Yet, the potential demonstrated by SAR sensors in monitoring forest disturbance caused by humans and fire makes their use compelling since insect outbreaks and windthrows influence forest structure similarly by changing the relative position and quantity (i.e., defoliation, fallen trees) of the vegetation material, and by changing the vegetation water content (i.e., drying up of affected trees). Such changes could influence the dominant scattering mechanisms, as well as signal attenuation through the vegetation layer. In the case of the L-band, cross-polarized radar scattering is largely the result of backscatter from large elements present in the forest canopies (i.e., branches, snags), and the foliage acts as an attenuation layer (Le Toan et al., 1992). The removal of the vegetation material or reduction in the vegetation water content is expected to decrease the cross-polarized radar scattering, with lower values being generally expected after disturbance events (i.e., reduced scattering due to decreasing scattering elements) not compensated for by reduced attenuation. For co-polarized waves, scattering from the ground plays a large role particularly when the vegetation layer is removed, which might hamper the retrieval of disturbed areas. The aim of this study was to evaluate the sensitivity of L-band data to changes in forest structure caused by wind and insect outbreaks.

The specific objectives were i) to evaluate the extent to which changes in forest structure caused by wind and bark beetle outbreaks influence the L-band SAR signal, ii) to understand the influence of pre- and post-disturbance SAR acquisition timing as well as of post-disturbance management practices on SAR backscatter changes, and iii) to estimate the accuracy of disturbance mapping using L-band SAR data.

Table 1
ALOS data used to evaluate forest disturbance caused by the windstorm Kyrill (windthrows) and bark beetle outbreaks. Information on precipitation (sum of three previous days, the acquisition day, and the following day), and minimum and maximum temperature at SAR acquisition date are also provided.

ALOS		Satellite pass (local time)	Acquisition dates	Grosser Arber meteorological station[a]	
Path	Frame			Accumulated precipitation (mm)	Min/max temperature (°C)
				Windthrows	
630	980	Ascending (21:15)	2006.09.30	2.2 (1.0**)	9.0/14.2
			2007.04.02	6.3 (1.9*, 4.3**)	1.5/6.6
			2007.05.18	26.6	−1.1/8.6
			2011.04.13	17.8 (8.1*, 0.7**)	−5.5/−2.8
				Insect outbreaks	
635	970	Ascending (21:30)	2007.08.11	17.6 (3.1*)	9.8/12.5
			2007.09.26	15.9 (12.0*, 0.4**)	1.8/4.6
			2008.06.28	0.2 (0.1**)	7.6/13.1
			2009.07.01	54.9 (16.0*, 26.0**)	11.4/17.7
			2010.05.19	6.5 (3.2*)	−1.1/0.9
			2010.07.04	6.3 (1.6*, 4.7**)	12.9/21.5
636	970	Ascending (21:30)	2007.07.13	36.5 (2.4*)	7.3/14.0
			2007.08.28	0.4 (0.4**)	6.8/12.5
			2007.10.13	0.6 (0.6*)	0.0/3.6
			2008.05.30	0.0	15.0/23.9
			2008.07.15	24.9 (2.5**)	6.2/12.5
			2009.09.02	11.6 (2.2*, 8.9**)	11.1/16.0
			2010.06.05	34.9 (3.7**)	9.0/18.1

[a] Source: Integrated Climate Data Center (ICDC), Hamburg University. *Precipitations (out of total) reported for the acquisition date (i.e., includes precipitations from 9 am on the previous day to 9 am on acquisition day) **Precipitations (of total) reported for the following day after image acquisition (i.e., includes precipitations from 9 am on the acquisition day to 9 am the following day; the actual image acquisition time falls within this interval).

2. Study area and data sets

The study was carried out in the Bavarian Forest National Park. The national park covers an area of 244 km^2 in southeastern Germany (Fig. 1) along the border with the Czech Republic. The area is mountainous, with elevation varying between 600 and 1453 m a.s.l. Mean annual temperature ranges between 6.5 °C in the valleys and 3 °C at higher elevations. Mean annual precipitation ranges from 830 to 2230 mm, a considerable amount of which occurs as snowfall (Heurich et al., 2010a). Snow cover persists for seven to eight months at higher elevations and for five to six months in valleys. Above 1100 m a.s.l. (16% of the area), sub-alpine spruce forests with Norway spruce and some common rowan (*Sorbus aucuparia*) prevail. Between 600 and 1100 m a.s.l. (68% of the area), mixed montane forests with Norway spruce, silver fir (*Abies alba*), European beech (*Fagus sylvatica*), and sycamore maple (*Acer pseudoplatanus*) are found. In wet depressions at the bottom of valleys (16% of the area), often associated with cold air pockets, spruce forests with Norway spruce, mountain ash, and birch (*Betula pendula*, *Betula pubescens*) predominate (Cailleret et al., 2014).

A major outbreak of spruce bark beetle started in the national park around 1995. The outbreak was attributed to both stand variables and large-scale drivers difficult to control by traditional forest management (Seidl et al., 2016). After the wind storm Kyrill (January 2007), which affected 412 ha, the total disturbed area reached about 7000 ha. Salvage logging took place in all areas except the core zone (Lausch et al., 2010). The extent of areas affected by insect outbreaks in the national park have been routinely mapped since 1988 using high-resolution aerial ortho-photographs acquired yearly between the end of July and the beginning of November (Heurich et al., 2010b). Since 2004, digital images at a spatial resolution of 20 cm have been acquired with an Intergraph Z/I Imaging Digital Mapping Camera (DMC), which uses three bands in the visible and near-infrared spectrum. The photograms are orthorectified and used to digitize the perimeter of areas seemingly affected by bark beetles. Only polygons containing at least five trees with visible damage are digitized. The extent of the areas affected by insect outbreaks (Fig. 1) is available as a vector file (39,318 polygons) and contains additional attributes, such as the year of detection and the type of intervention (i.e., clearing, no intervention, and dead trees present on the ground). A subset of this layer (3576 polygons with areas between 0.1 and 22.0 ha) was extracted for a period matching the available SAR images (2007–2011). This subset forms the reference vector layer for insect outbreaks. The minimum limit of 0.1 ha was used as it roughly matches the spatial resolution (30 m) of the processed SAR datasets. Locations of trees toppled by the storm Kyrill were digitized on the DMC image acquired on September 16, 2007 and saved as a vector file (Heurich et al., 2010b). The vector layer contains information on the affected areas and management interventions (clearing vs. no intervention) after the storm. A subset of this vector layer (423 polygons with an area between 0.1 and 10 ha) was used. This subset forms the reference vector layer for windthrows. These reference vector layers were used to extract samples (i.e., pixels) for all subsequent analyses.

The analysis was conditioned by the availability of SAR data sets because acquisitions from the same satellite orbit are needed before and after disturbance to allow for pixel-based comparisons. Only advanced land-observing satellite (ALOS) phased array-type L-band synthetic aperture radar (PALSAR), fine beam dual (FBD), and polarimetric (PLR) acquisition modes were considered due to their high spatial resolution and the availability of the cross-polarized (HV) channel. High spatial resolution was needed to account for spatial heterogeneity of disturbances. The cross-polarized channel was deemed necessary based on earlier results that showed its sensitivity to forest structural characteristics and their change (Joshi et al., 2015; Mermoz and Le Toan, 2016; Tanase et al., 2015b; Tanase et al., 2014). SAR data were provided by the Japanese Aerospace Exploration Agency (JAXA) in single-look complex (SLC) format. Four PLR images were used to derive change ratios (post-event divided by pre-event backscatter values) for dates corresponding to the windstorm Kyrill. The effects of insect outbreaks were evaluated using 13 dual-polarized (HH, HV) FBD datasets available from two orbital paths (i.e., 635 and 636). The datasets were acquired with an incidence angle at swath center of 24° and 39° for PLR and FBD modes, respectively. The acquisition dates together with the environmental conditions at acquisition are presented in Table 1. Information on accumulated precipitations aided in the interpretation of the results. Accumulated precipitation provides an indication of the environmental conditions at image acquisition; datasets acquired during stable, dry periods showed improved sensitivity to forest structure in a range of environments from Mediterranean to boreal (Cartus et al., 2012; Kalogirou et al., 2014; Lucas et al., 2010; Tanase et al., 2010). For temperate environments, the spatial variability of soil moisture in the top few centimeters should be low during summer due to high air temperatures and low precipitations. Therefore, accumulated precipitation for an interval prior to the SAR acquisition should more closely reflect overall environmental conditions (dry vs. wet).

3. Methods

3.1. SAR data processing

ALOS PALSAR data acquired on the same orbital path were co-registered using as reference the first image of each data series and a cross-correlation algorithm (Werner et al., 2005). After co-registration, each image was multi-looked in range and azimuth to obtain a ground pixel spacing of approximately 30 m. The high resolution was necessary

to allow preservation of the localized influence of disturbance events and thus to avoid errors in SAR signature analysis. The use of high-resolution SAR data might also help to minimize omission errors, particularly along disturbance borders (Santoro et al., 2012). PLR images were multi-looked by 1 (range) and 9 (azimuth); FBD images were multi-looked by 2 (range) and 10 (azimuth). SAR intensity was transformed to the radar backscatter coefficient after applying polarization-specific absolute calibration factors (Shimada et al., 2009). The backscatter coefficient (γ°) was normalized using the real scattering area derived at the pixel level (Frey et al., 2013) using the digital elevation model (25 m) over Europe (Bashfield and Keim, 2011). Multi-temporal filtering was applied to decrease speckle (Quegan et al., 2000). The final SAR pre-processing step was orthorectification to the Universal Transverse Mercator (UTM) projection using a look-up table based on the SAR orbital information and the digital elevation model (Wegmüller et al., 2002). The equivalent number of looks after processing was, on average, 27 for the FBD data and 13 for the PLR data; the standard deviation of the backscatter coefficient over stable forested areas ranged between 0.8 and 1.2 dB, depending on polarization and image date. The low equivalent number of looks did not affect signature analysis as hundreds of pixels were grouped to derive the average values and confidence intervals (CI). Radar change ratios (RCR) were computed (Eq. (1)) using pre- and post-disturbance averaged backscatter to better represent the typical forest condition by removing the stochastic part of the signal. The rationing of radar intensities is better adapted to the statistical characteristics of SAR data than the intensities subtraction (Rignot and Zyl, 1993). More details about RCR in the form of the equivalent radar burn ratio (RBR) can be found in Tanase et al. (2015a, 2015b).

$$RCR_{xy} = Post_{event}\overline{\gamma^0}_{xy} / Pre_{event}\overline{\gamma^0}_{xy} \quad (1)$$

where xy represents a specific radar polarization (i.e., HH, HV, or VV), and $\overline{\gamma^0}$ represents the multi-temporal average backscatter coefficient at pixel level.

Since post-event to pre-event indices are sensitive to changes in forest structure, a priori, they should be sensitive to changes resulting from causes other than fire or logging, as demonstrated in the following sections. For undisturbed forests, multi-temporal backscatter averages provide more accurate values by filtering out random temporal variations, as forest structure is largely stable, but backscatter values might fluctuate due to changes in soil moisture or vegetation water content. In disturbed forests, the backscatter signal is affected not only by the remaining vegetation, but also by recovery processes, such as recruitment and regrowth. However, for temperate coniferous forests, regrowth is slow (Zeppenfeld et al., 2015). Since L-band backscatter is mostly influenced by large vegetation components, such as branches and trunks (Le Toan et al., 1992), recruitment has limited influence on the post-event radar signal in the first years after disturbance.

3.2. Windthrow analysis

SAR values for each polarization (i.e., σ°_{HH}, σ°_{HV}, σ°_{VV}) and acquisition date were extracted for pixels located within the polygons digitized as affected by the storm Kyrill. Ten large polygons were added to the reference vector layer through the digitization of areas seemingly not disturbed over the past years. Such areas were identified using recent optical imagery (Google Earth and Bing Aerial layers) and were used to estimate backscatter change in undisturbed forests. A total of 6053 pixels (2725 affected by wind and 3328 not affected) were extracted and used for statistical analyses of the backscatter trends and to compute the threshold values separating affected areas from stable, unaffected ones.

RCR values were computed for each polarization using the single pre-event dataset available. For each RCR, the mean, median, standard deviation, and CI (95%) were estimated. The dynamic range, i.e., difference between average pixel backscatter of disturbed and undisturbed areas, was used as an indicator of index sensitivity to forest structural changes (Cartus et al., 2012). The mean and median RCR values of areas affected by wind were compared to those of unaffected areas. Furthermore, the mean (and CIs) and median values were analyzed as a function of the post-event management interventions (no intervention vs. salvage logging) and environmental conditions at image acquisition. Based on the observed trends, average values, CIs, and the dynamic range, thematic maps showing windthrows location were derived. The maps were based on thresholds on the HV backscatter change for the datasets acquired in April 2007 and 2011, relative to the dataset acquired before the storm (0.6 dB and −1.8 dB, respectively). The thresholds were derived by averaging median values observed for affected and unaffected areas.

Derived maps were validated using an independent dataset. The independent dataset was obtained by randomly selecting pixels affected by wind out of an initial set of pixels falling within the boundaries of the reference vector layer. The sampling size for validation was computed according to Eq. (2) (Olofsson et al., 2014). A stratified random sampling design was selected; the number of samples for the disturbed strata was computed according to Eq. (3); the number of samples for the undisturbed strata were obtained as the difference between the total number of samples and the samples of the disturbed strata.

$$n = \frac{(\sum w_i S_i)^2}{[S(O)]^2 + (1/N)\sum w_i S_i^2} \quad (2)$$

where S(O) is the expected standard error for the overall accuracy, W_i is the class proportion, S_i is the standard deviation of stratum i (as described by $Si = \sqrt{U_i(1-U_i)}$, where U_i is the expected user accuracy), and N is the sampling population. When N is large, the second term in the denominator can be ignored.

$$V(U_i) = U_i(1-U_i)/(n_{af}-1) \quad (3)$$

where U_i is the expected user accuracy, $V(U_i)$ is target variance for the user accuracy, and n_{af} is the number of samples to extract in the affected area.

The following assumptions were used to derive the number of samples: i) proportion of disturbed area 2% (i.e., mean area disturbed yearly by wind and insect outbreaks within the national park for the period 2007–2011, obtained from the reference vector layer), ii) expected user accuracy for affected areas, 60%, iii) expected user accuracy for unaffected areas, 80%, iv) standard error for the overall accuracy expected, 0.01, and v) target variance for the user accuracy, 0.0005. Confusion matrices were formed using the affected and unaffected pixels; overall, user, and producer accuracies were computed to evaluate the results.

Practically, all pixels falling within the affected polygons were extracted and 488 of them (sampling size for disturbed areas validation) were randomly selected for validation (the remaining 2725 pixels were used for analyses and calibration). In addition, 934 pixels (sampling size for undisturbed areas validation) were selected at random locations in areas not affected by the storm Kyrill. The coordinates of the 1422 randomly selected pixels were joined to form the validation layer for windthrow mapping.

3.3. Insect outbreak analysis

Areas affected by insect-related disturbances were matched with ALOS FBD polarized (σ°_{HH}, σ°_{HV}) datasets according to the outbreak detection date (ODD) and the post-event SAR image acquisition date. The ODD for the three years analyzed was August 31, 2008; August 20, 2009; and August 22, 2010. As for windthrows, the analysis focused on the statistical properties of areas affected by beetle outbreaks compared to those of unaffected areas. The number of pixels used for analyses is presented in Table 2. For validation purposes, sets of random pixels

Table 2
Number of pixels used to compute mean and median values by year of outbreak (example). The average of all pre-event images acquired was used (i.e., 'Mean 2007').

	Outbreak year					
sRCR ratio (path/frame)	2007	2008	2009	2010	2011	Not affected[a]
2008.06.26/mean 2007 (635/970)[b]	1719	1114	1862	1508	609	478
Mean 2008/mean 2007 (636/970)[c]	1745	1002	2042	1688	830	482

[a] Reference pixels extracted within the polygons added in areas without outbreaks.
[b] Pixels marked as 'cleared' for year 2007 were eliminated.
[c] Pixels marked as 'cleared' for years 2007 and 2008 were eliminated.

were selected by year of disturbance from the pool of all affected pixels. The validation datasets were generated for each year between 2007 and 2010. The number of validation samples was computed as described in the previous section. For affected areas, between 484 and 496 pixels were used for validation depending on disturbance year. Unaffected areas were validated using 1085 (for ALOS path 635) and 1031 (for ALOS path 636) random pixels selected in areas not affected by insect outbreaks over the analyzed period.

Since the study area was contained within different SAR frames, the RCR values were standardized (sRCR). sRCR might be useful when study areas extend over several orbital paths to account for variable environmental conditions at image acquisition (Tanase et al., 2015a, 2015b). Standardized values were computed using the mean and standard deviation of unaffected areas for each image ratio analyzed (4).

$$sRCR = (RCR - \mu RCR)/\sigma RCR, \quad (4)$$

where RCR is the backscatter ratio to normalize, and μRCR and σRCR are the mean and standard deviation of RCR, respectively, over forested areas not affected by disturbance.

Backscatter values are the result of an interplay between forest structure, vegetation water content (often related to forest health), and other factors, such as environmental conditions at image acquisition (e.g., precipitation, temperature) and surface properties (moisture and roughness). The original index (i.e., RBR) was designed and used to assess point time events (i.e., fires). To reduce variable environmental conditions at image acquisition, around ten images were used to compute average pre- and post-event states according to Tanase et al. (2015b). Such an approach is less feasible for temporally dynamic processes, particularly when only few images are acquired every year. Furthermore, ALOS FBD acquisitions are scheduled between spring and autumn (i.e., beetle outbreaks gradation), meaning that the images were acquired at various stages during the attack (i.e., green, red, gray). To limit the influence of variable forest conditions, caused by the continuous nature of the outbreaks and human interventions, the post-event means were computed over short periods (e.g. one summer) when only few images (up to three) were available (Table 1). Datasets acquired under extremely wet conditions (2009.07.01) or at freezing temperatures (2009.05.15) were removed from the analysis as it has been demonstrated that such events might diminish SAR sensitivity to forest structure (Cartus et al., 2012; Lucas et al., 2010; Santoro et al., 2002; Tanase et al., 2010; Thiel et al., 2009). Another factor considered when deciding which images are useful for temporal averaging was the acquisition date relative to the bark beetle phenology. For example, when analyzing the 2008 event (using 2009 post-event data), one needs to exclude from pre-event averaging the image acquired in July (2008.07.15) as bark beetles might have already caused significant damage.

All possible combinations of post- to pre-event ratios were analyzed (i.e., post-event to each pre-event image ratio, post-event to average pre-event images, and post-event average to pre-event average) to assess the influence of the environmental conditions and acquisition timing relative to the bark beetle phenology. The analysis was carried out for each year between 2007 and 2010. Pixel values were extracted using the reference vector layer and analyzed depending on the SAR acquisition and outbreak detection dates. Pre-event images were selected if acquired one year before outbreak detection. As such, it was possible to analyze insect attacks at ODD − 1 (i.e., before the detection year specified in the reference vector file), ODD (during the detection year, when the post-event image was acquired late summer or autumn) and ODD + 1 (areas identified as attacked the following year in the reference vector file).

Polygons marked as 'no intervention' were typically used to extract the SAR signatures because detection of logging activities was beyond the scope of this study. Salvage logging after bark beetle outbreaks can occur the entire year and starts after the first swarming of the beetles when temperatures reach about 20 °C degrees in spring (Wermelinger, 2004a). After salvage logging, old spruce trees are removed, but some regeneration and beech trees can remain. Inclusion of cleared areas in the analysis would have artificially increased the perceived sensitivity to insect-related disturbance because logged areas show lower backscatter levels than disturbed forests (i.e., dead or dying trees on site remain significant scattering elements until they are completely dried out). However, polygons marked as 'cleared' were also used when bark beetle attacks were detected past the acquisition date of the post-event SAR image (i.e., salvage logging was carried out after the satellite pass). In such cases, it was considered that at SAR image acquisition, trees were still present on site. Table 3 provides information relating post-event images to the analyzed polygons as a function of outbreak detection date. As pre-event image, all datasets acquired before the detection year and their average (except for images acquired under heavy rainfall and freezing conditions) were used. The pixels used for statistical analysis were extracted only if located within the affected polygon boundaries to limit the mixing of different forest conditions (affected vs. unaffected). Ten polygons were added through digitization of areas seemingly not disturbed over the past years. The number of pixels available for the analysis depended on the post-event image acquisition date, as areas marked as 'cleared' might have been excluded for some years (Table 3).

Between 609 and 2042 pixels were available for the analysis for any

Table 3
Polygons used for statistical analysis as a function of SAR image acquisition date. Areas without intervention are marked as 'no int.'. Areas marked as 'cleared' were eliminated depending on post-event SAR dates.

Path/row	Pre-event images	Post-event image	Areas considered for analysis by outbreak year		
			Pre-event outbreak	Same year outbreak	Post-event outbreak
635–970	2007.08.11, 2007.09.26	2008.06.28	2007 (no int.)	2008 (all)	2009–2011 (all)
	2007.08.11, 2007.09.26, 2008.06.28	2010.07.04	2009 (no int.)	2010 (all)	2011 (all)
	2007.07.13, 2007.08.28, 2007.10.13	2008.05.30	2007 (no int.)	2008 (all)	2009–2011 (all)
	2007.07.13, 2007.08.28, 2007.10.13	2008.07.15	2007 (no int.)	2008 (no int.)	2009–2011 (all)
636–970	2007.07.13, 2007.08.28, 2007.10.13, 2008.05.30	2009.09.02	2008 (no int.)	2009 (no int.)	2010–2011 (all)
	2007.07.13, 2007.08.28, 2007.10.13, 2008.05.30, 2009.09.02	2010.06.05	2009 (no int.)	2010 (all)	2011 (all)

given sRCR ratio and ODD. A set of thresholds was applied to the most sensitive RCR indices to classify the area as 'no change' or 'insect outbreak'. Three types of thresholds were tested: i) −1.0 dB, based on the average maximum dynamic range (regardless of insect outbreak detection year), ii) −0.7 dB, based on the average dynamic range of areas affected during the year of SAR image acquisition (areas affected in previous or subsequent years were not considered), and iii) −0.5 dB based on the radiometric accuracy of the ALOS PALSAR sensor (Shimada et al., 2014). The first two thresholds were computed as the average of the median values for disturbed and undisturbed forests. The latter threshold was used as it provides an approach based on sensor radiometric sensitivity. Validation of affected vs. unaffected areas was carried out using the set of randomly selected pixels and confusion matrices.

4. Results

4.1. Windthrows

As expected, lower RCR values were observed over wind-affected areas than over unaffected areas at all polarizations. This pattern was the result of decreased post-disturbance backscatter levels over affected areas. A decrease in magnitude depended on environmental conditions at image acquisition and time since event. For HH and HV polarizations, RCR indices indicated statistically significant changes (i.e., no overlap between CIs) compared to pre-event conditions, except for the dataset acquired under wet conditions (2007.05.18). For VV polarization, significant backscatter changes over wind-affected areas appeared only for the last image, acquired four years after the event (2011.04.13). Distributions of RCR values were normal over all polarizations and images analyzed. The interval of RCR values (pixel level) was wide and non-outlier ranges largely overlapped (Fig. 2, lower panels). Such wide intervals are expected when working at high resolution (i.e., low number of looks) due to the coherent nature of the SAR signal (constructive and destructive interference, which results in speckle). Since the mean values by classes were computed over many pixels, such interferences were filtered out, thereby providing stable mean and CI values. The variable RCR values over stable (unaffected) areas are the result of variations in environmental conditions at the acquisition of post-event datasets, as the same pre-event dataset was used (Fig. 2).

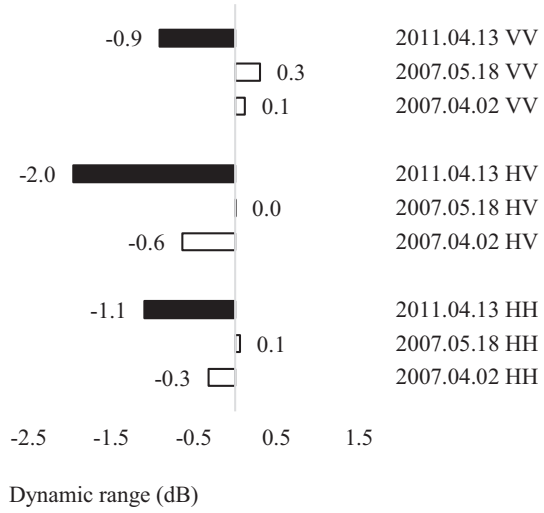

Fig. 3. Dynamic range of RCR indices for each post-event image acquisition date. Filled bars show the dynamic range for the image acquired four years after the disturbance event (i.e., affected trees were likely removed from site). HH, horizontal transmit/receive; HV, horizontal transmit/vertical receive; VV, vertical transmit/receive.

The amount of change (dynamic range) associated with each RCR, i.e., the difference in dB between the RCR of affected and unaffected areas, for all post-event datasets varied between 0 dB and 1.96 dB, depending on environmental conditions and polarization (Fig. 3). For all polarizations, the dynamic range observed for the SAR dataset acquired three months after the event was low (0.1 to 0.6 dB); the highest values were observed for the dataset acquired four years later. For the image acquired immediately after the event, only the HV polarization showed a dynamic range above the ALOS PALSAR calibration error (0.5 dB). Areas affected by windthrows were mapped using the HV polarization and the images acquired in April 2007 and 2011. The overall map accuracy was 69% when the dataset acquired in April 2007 was used and increased to 84% when the dataset acquired in 2011 was used; for affected areas, user and producer accuracies were above 54% and 67%,

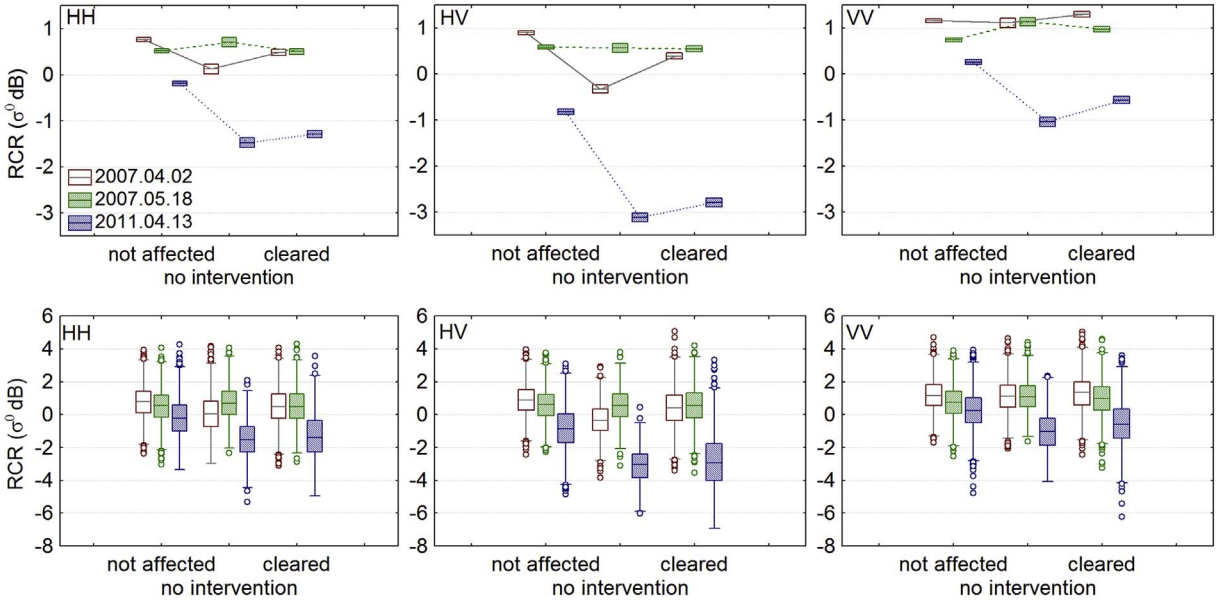

Fig. 2. Mean and median radar change ratio values from wind affected areas. Upper panels show the mean values computed for each post-event (windthrows) image and SAR polarization, together with confidence intervals. The mean backscatter is shown as horizontal lines; CIs (95%) are represented by box edges. Lower panels show median values (horizontal line), percentiles (25% and 75%, box edges), non-outlier values range (whiskers), and outlier values (circles). Differences between management types (i.e., no intervention, cleared areas) are also shown. HH, horizontal transmit/receive; HV, horizontal transmit/vertical receive, and VV, vertical transmit/receive.

Table 4
Validation results (%) for windthrow mapping using different post-event images and HV polarization.

Classification accuracy	2007.04.02		2011.04.13	
	Affected	Unaffected	Affected	Unaffected
User	54	80	75	89
Producer	67	70	81	86
Overall	69		84	

respectively (Table 4). Machine-learning classification techniques (results not shown) rendered similar overall accuracies (within 2%), even when multiple independent variables (i.e. polarizations) were used.

4.2. Insect outbreaks

Five pre-event and eight post-event datasets were analyzed to assess sRCR sensitivity to insect-related disturbances. Of the eight post-event datasets, two were acquired under sub-optimal conditions (2009.07.01 and 2010.05) and were only used to evaluate the extent to which such conditions influence the discrimination between affected and unaffected areas (i.e., not for temporal averaging or thresholds computation). Statistically significant differences were observed for areas marked as outbreaks before the post-event SAR image date when compared to unaffected areas (Fig. 4). Stable areas showed sRCR values close to 0 (no change). Increasing effects on forest structural parameters resulted in increasingly negative values of the standardized RCR (post-event values lower than pre-event values). Analysis of all available datasets indicated that a threshold of −1.0 dB is a consistent indicator of forest structural changes induced by bark beetle attacks. sRCR values between 0 and −1 indicated lower intensity changes with respect to the reference date, which might be related to the onset of the outbreaks (see values for polygons marked as affected after the analyzed post-event SAR image; Fig. 4).

Outbreaks recorded in the previous year (e.g., 2007, for the post-event image acquired in 2008; Fig. 4 upper left panel) have sRCR values around −2 dB, whereas on-going outbreaks (i.e., 2008) have slightly higher sRCR mean values. One should note that the SAR acquisition date in 2008 was in early summer (June 28), which might explain the smaller changes for the areas affected in 2008 compared to the reference dataset (large parts of affected trees might still be alive, as opposed to the end of summer, when these trees are mostly dead). More interesting, however, were the mean values (and CIs) recorded for areas identified as affected in the air-borne flight from 2009 (i.e., after ALOS acquisition date in 2008). Such areas were characterized by statistically different sRCR values compared to the areas affected by insect outbreaks in following period (2010−2011). This suggests that although these areas were not identified as affected in the 2008 air-borne flight (August 31), some processes (e.g., declining tree health) were already on-going by the end of June. Such early detection capabilities were confirmed for other dates (2011 in the upper right and 2010 in the lower middle panels in Fig. 4). In both cases, areas detected as affected in the air-borne flights following the SAR acquisition date (2011 and 2010, respectively) showed negative changes that might be associated to the onset of the outbreak.

Choosing the right pair of images to compute sRCR values when environmental conditions varied over short periods was complex (Fig. 5). When individual image-to-image (as opposed to mean-to-mean) sRCR ratios were considered, higher dynamic ranges were observed, particularly when the image acquired under wet conditions on July 13, 2007 was used as reference (Fig. 5, left most panels). Indeed, for the remaining combinations, it seemed considerably more difficult to adequately discriminate affected areas, as most values were close to 0 dB (no change). Such a lower discrimination capacity seems to be related to the drier conditions of the reference datasets (2007.08.28 and 2007.10.13) as opposed to the wetter conditions for the remaining images. Under dry conditions, some decrease in the forest backscatter is expected due to the decreased vegetation water content. Thus, the decrease in backscatter caused by bark beetle infestation seems to have been compensated for by the lower initial reference levels, with most values hovering around or above the no-change threshold (0 dB).

Management interventions affected RCR values such that areas affected by salvage logging exhibited lower post-event backscatter values

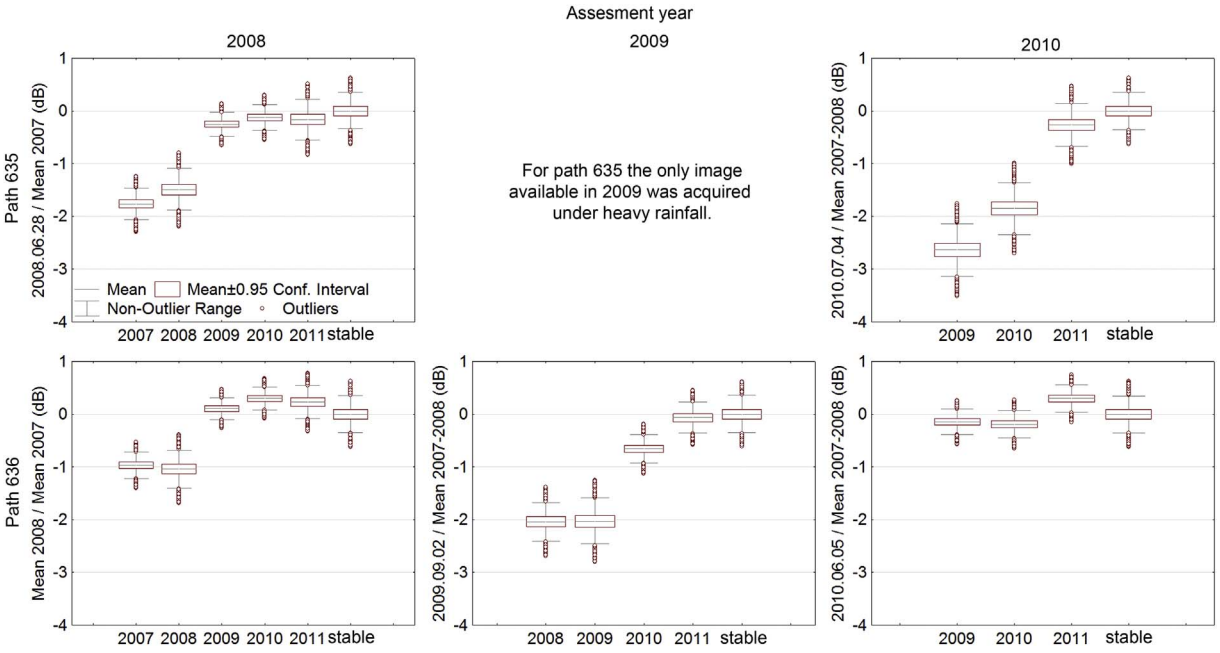

Fig. 4. Mean sRCR values and CI (95%) for areas affected by bark beetles per year compared to that of stable areas (unaffected). Note that outbreaks detected after the specified post-event image used might be distinguished for some of the sRCR ratios (lower values when compared to subsequent years). The ordinate axis shows sRCR values (for the specified post-event and pre-event pairs) extracted in polygons marked as affected in different years (abscissa values). Average values of datasets acquired before the event were used (e.g., 'Mean 2007', 'Mean 2007–2008').

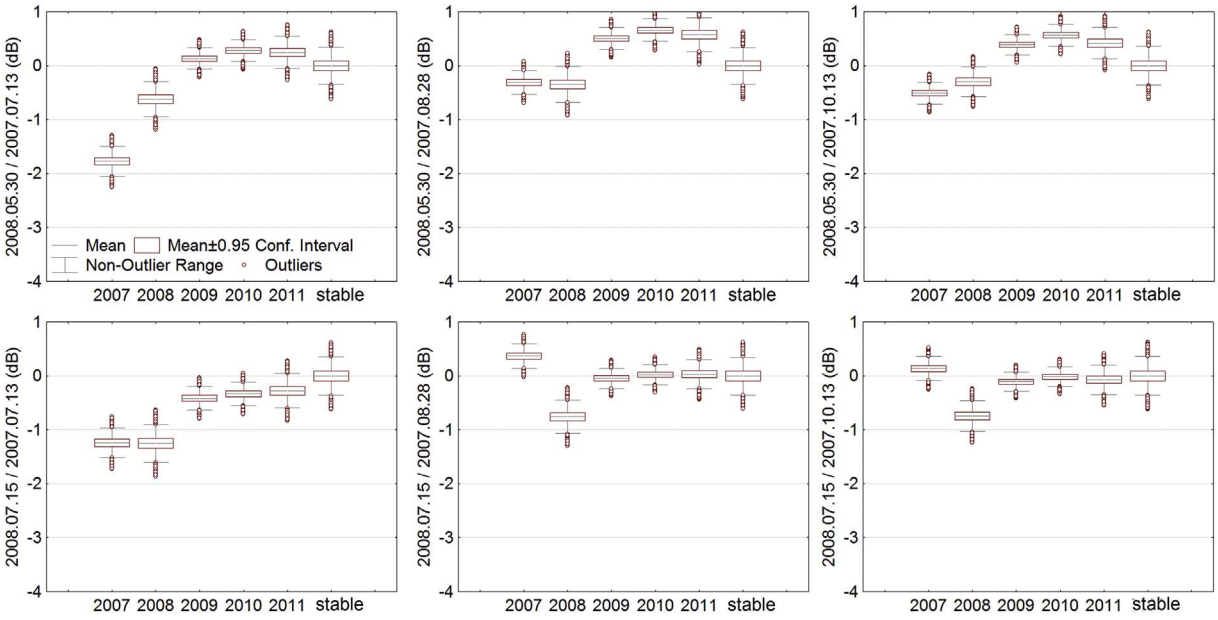

Fig. 5. sRCR values for different combinations of post-event to pre-event ratios per year. Examples are given for assessment year 2007 using ALOS PALSAR FBD data from path 636. Areas affected over the following years (2008–2011) are also displayed.

(Fig. 6). When compared to areas with no intervention, such differences were particularly large (4.5 dB) for some years (2009). Conversely, for 2010, the differences were small and not statistically significant.

The overall classification accuracy varied between 64% and 91%, depending on the outbreak detection date and the sRCR index (Table 5). Note that the accuracy was assessed using the reference polygons identified as affected in the previous, current, and past year with respect to the acquisition date of the post-event SAR data used. The lowest overall accuracies (64–74%) were observed for areas affected by outbreaks in the year following the acquisition of the post-event SAR image, which might correspond to the detection of the onset of the outbreak. Areas affected by insect outbreaks in previous and current post-event SAR image acquisition were classified with overall accuracies ranging from 74% to 91% depending on the image pair. Classification using support vector machines (results not shown) rendered overall accuracies values within 1% of the thresholding approach.

The use of different thresholds had a small effect (± 3%) on the overall accuracy (Fig. 7). However, changing the threshold had a considerable influence on how omission and commission errors varied between classes. For areas affected by bark beetles, commission errors were lowest (15% on average) when the disturbance occurred before the post-event SAR acquisition date (−1.0 dB threshold), whereas omission errors were considerable larger (60% on average). When the threshold was increased to −0.5 dB, commission errors increased (by 4% on average), whereas omission errors decreased (by 6% on average).

Areas not affected by bark beetles were classified more accurately, with average commission errors between 19% and 16%, depending on the threshold used. Omission errors for undisturbed areas were rare, with average producer accuracy ranging between 92% and 97%, depending on the threshold. When thresholds were changed from −1.0 to −0.5 dB, the tolerance to different types of errors was controlled. Balanced omission and commission errors were achieved for the −0.5 dB threshold (Table 5 and Fig. 7).

5. Discussion

For both disturbance types, the cross-polarized channel showed the highest sensitivity to changes in forest structure, and a simple mapping approach based on thresholds produced results similar to those of more advanced machine-learning algorithms (results not shown). Classification accuracies were largely in line with those of previous studies (Ortiz et al., 2013; Ranson et al., 2003; Schwarz et al., 2003). For some datasets, areas susceptible to bark beetle disturbance were identified (at lower accuracies) with about one-year lead time when compared to the reference dataset. By adopting a change-detection framework, distinct advantages were tapped: i) removal of topographic

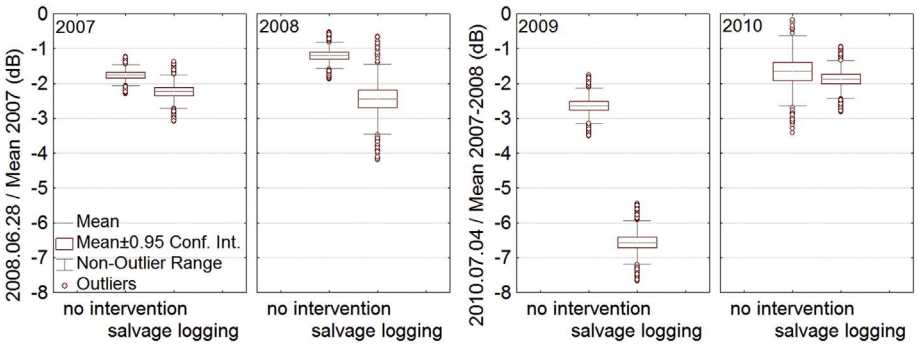

Fig. 6. The influence of salvage logging (clearing of trees) on sRCR values. The two panels on the left show areas affected by bark beetle outbreaks in 2007 and 2008 as seen in the data acquired in June 2008. The two panels on the right show areas affected in 2009 and 2010 as seen in data acquired in July 2010.

Table 5
Validation results (%) for insect disturbance mapping (HV polarized data). An example is given for outbreaks detected in the previous, current, and subsequent years as compared to the post-event SAR acquisition date. A threshold of −0.5 dB was used for classification.

sRCR index	Outbreak detection year	Accuracy (%)				
		Affected areas		Unaffected areas		Overall
		User	Producer	User	Producer[a]	
2008.06.28/ mean 2007 (path 635)	2007	68	62	84	87	79
	2008	65	55	82		77
	2009	41	21	71		67
	2007–2008	80	59	70		74
Mean 2008/ mean 2007 (path 636)	2007	59	28	77	92	74
	2008	63	32	77		75
	2009	21	4	67		64
	2007–2008	76	30	63		65
2009.09.02/ mean 2007–200-8 (FBD path 636)	2008	77	78	91	91	87
	2009	83	92	96		91
	2010	68	40	76		74
	2008–2009	89	85	88		88
Mean 2010/ mean 2007–200-8 (path 635)	2009	92	74	89	97	90
	2010	84	33	76		77
	2011	48	6	69		69
	2009–2010	94	54	70		77

[a] The same accuracy is the result of using a unique dataset as reference for areas unaffected by disturbance.

effects, a predominant factor influencing radar scattering, and ii) increased signal-to-noise ratio using multi-temporal averages.

5.1. Windthrows

Statistically significant changes in backscatter were recorded for areas affected by windthrows. The highest dynamic range between affected and unaffected areas was observed for images acquired under freezing conditions, but one should consider that post-event images acquired under dry conditions were not available. Rainfall negatively influenced the capacity of SAR data to detect changes between acquisition dates. As for other disturbance types, such as logging and fire (Joshi et al., 2015; Mermoz and Le Toan, 2016; Tanase et al., 2010), the highest sensitivity to forest structural changes was observed for the cross-polarized channel. High backscatter changes generally corresponded to areas affected by windthrows. The overall mapping accuracy (69–84%) was in line with previous results (88%) based on manual interpretation of air-borne X-band interferometric coherence (Schwarz et al., 2003). The user accuracy for the affected areas was lower for this study (54% to 75% vs. 93%) when compared to the study of Schwarz et al. (2003), but the producer accuracy was higher (67–81% vs. 35%), which indicates different tolerances to commission and omission errors between the two retrieval algorithms. The lack of quantitative reporting for the other studies available (Eriksson et al., 2012; Fransson et al., 2010; Fransson et al., 2002; Green, 1998) precluded similar comparisons.

Schwarz et al. (2003) found that L-band amplitude data was not sensitive to windthrows—a conclusion in contrast with our results. Furthermore, Green (1998) found that co-polarized channels were more sensitive to gaps than were cross-polarized channels, which again leads to the opposite conclusion. Such differences might be explained by the use of change-detection approaches instead of the single-date post-event analysis in the aforementioned studies. Our results were more in line with those of Fransson et al. (2002), who demonstrated the utility of long-wavelength SAR (HH polarized, VHF 20–90 MHz) data for the detection of storm-damaged forests. However, the sensitivity of co-polarized channels to windthrows was observed only for images acquired long after the event (four years), and this sensitivity is most likely related to the decreased water content of the remaining trunks (i.e., the scattering from dry vegetation is lower). On the short term (3 months past event), the co-polarized channels were insensitive to windthrows, which support findings of earlier studies (Fransson et al., 2010; Schwarz et al., 2003). The low short-term sensitivity might be explained by the interaction of co-polarized waves with vertical or horizontal elements (i.e., tree trunks, branches) present after the event. After the windthrow, trees lie on the ground and still have their complete needles, branches, and trunks. Moreover, the trees are uprooted, and the root plates stand vertically up to several meters. The trees are still connected to their intact roots and are therefore provided with water. Over the

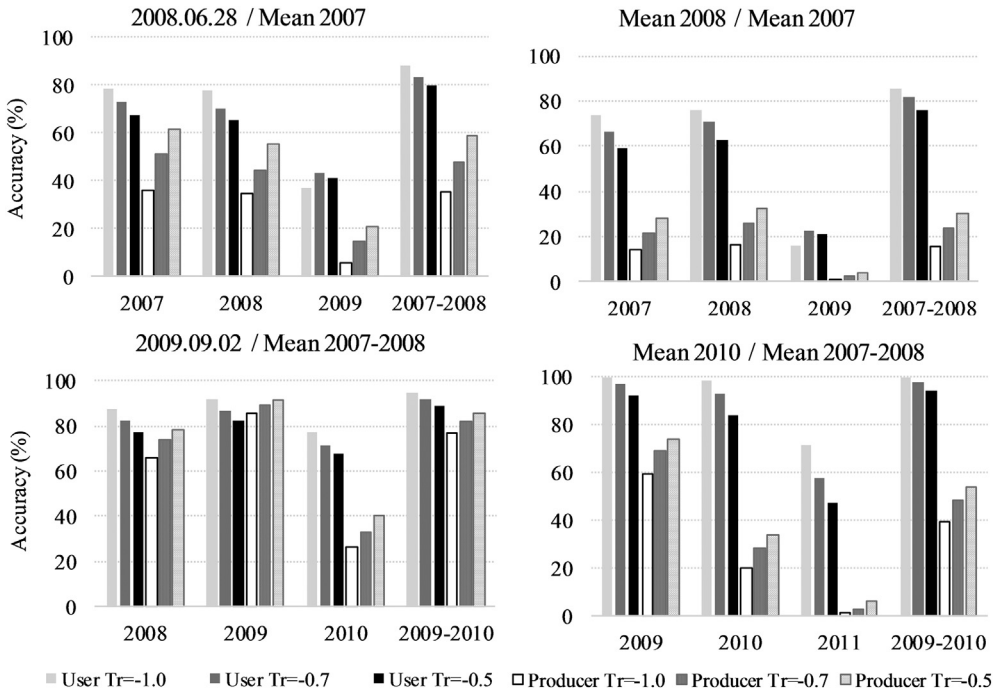

Fig. 7. User and producer accuracies as a function of the threshold (Tr) used (−1.0, −0.7, and −0.5 dB) to map areas affected by insect outbreaks.

following seasons, these trees will die, but their vertical structure remains (root plates, trunks laying in a network of several meters with branches and without needles). Because of snow and decay, the trunks will be pressed to the ground, and the branches will fall gradually; these structures will thus have less influence on the backscatter coefficient. Such reasoning might explain the increased sensitivity for the image acquired in 2011 (i.e., after the trees were most likely removed or dried up).

The rather small overall dynamic range observed immediately after the event for the HV polarization (0.9 dB) might be explained by the acquisition conditions of the individual datasets (i.e., spring). Particularly the second dataset (2007.05.18) was acquired after rainfall events (Table 1). Such conditions might affect the discrimination power, as also shown for other natural disturbances and for cross-polarized channels. The maximum observed dynamic range (−2 dB) was lower than values recorded after other types of natural disasters (−3 dB for areas affected by fires). The difference might be explained by residual backscatter from unaffected vegetation present within the affected pixels (e.g., live standing trees, toppled trees on the ground, understory vegetation).

It is difficult to explain the unexpected trend observed when 'cleared' and 'no intervention' areas were analyzed (Fig. 2). Similar trends were recorded for all backscatter channels except for the image acquired under wetter conditions (May 2007). In 'cleared' areas, one expects backscatter to decrease more (lack of vegetation material) than the backscatter of 'no intervention areas' (dead trees standing/laying). For the image acquired in April 2007, the opposite trend, particularly for HV polarization, might be related to wind impact levels as logging operations started later. It seems that areas with lower impact levels were marked for salvage logging, which might be consistent from an ecological perspective (i.e., to stop the bark beetle infestation). An alternative explanation might be related to the differentiated effect of the topographic slope on backscattering when vegetation structure changes. For the image acquired in 2011, the difference between the two treatments was minimal as expected; in areas marked for clearing, vegetation was removed, whereas in 'no intervention' areas, the standing trees dried up.

The higher map accuracies observed for the 2011 image were likely related to the increased dynamic range caused by tree removal or dried vegetation. Therefore, the resulting map was transformed into a forest vs. non-forest map. In such cases, very high accuracies are obtained using L-band data, as demonstrated in an earlier study (Shimada et al., 2014). The maps obtained using empirical thresholds were reliable; their accuracies were only slightly lower (2%) than maps obtained using machine-learning algorithms, such as SVM classification (results not shown).

Several limitations affected our study, particularly the SAR density of observations. The lack of pre-event acquisitions precluded the use of FBD datasets, a mode more frequently used within the ALOS PALSAR basic observation scenario. Therefore, a more detailed analysis of the influence of changing environmental factors was not possible. In addition, the lower spatial resolution of PLR datasets did not allow efficient multi-looking and thus did not allow speckle reduction, despite multi-temporal filtering. The availability of datasets with higher spatial resolutions should allow more accurate mapping by reducing miss-detection along borders (Santoro et al., 2012) and by identifying shadowing effects that might be used for identification of the areas affected by storm (Eriksson et al., 2012).

5.2. Insect outbreaks

The highest sensitivity to insect-related disturbance was observed for the cross-polarized channel (HV). The co-polarized channel (HH) showed a smaller dynamic range, which might be explained by the higher sensitivity of the HH polarization to the surface properties. Over affected areas, soil surface properties (roughness and moisture) play an increasing role in the scattering process because tree scattering is lower at a lower water content. In addition, defoliation after outbreaks removes the attenuation layer, which in turn allows a higher interaction of the incoming waves with the soil surface. Thus, over previously affected areas, temporal signal variation is higher than that of dense forests because soil surface properties have a larger influence on the scattering properties. Such areas should be masked out in a temporally iterative detection algorithm.

Salvage logging had a significant influence on backscatter. The extent to which salvage logging was completed could be assessed by the relative differences in sRCR values compared to areas marked as no-intervention. For example, for areas affected by bark beetles in 2007, salvage logging might have still been on-going in June 2008 (note the small difference in mean values between areas marked as no intervention and areas marked as cleared in Fig. 6). By contrast, for the 2009 outbreak, salvage logging seems to have been completed by July 2010 as the difference to the no-intervention areas was substantial.

Backscatter changes generally corresponded to bark beetle outbreaks, as shown by the generally low commission errors (6–24%) observed for the affected class. The values were lower than those of an earlier study (75%) based on X-band data alone (Ortiz et al., 2013). Omission errors for the affected class (around 45%) were also lower than X-band results (47%), but to a lesser extent. The average overall accuracy computed for areas affected in the previous and current year (as a function of the post-event SAR acquisition date) was about 10% lower than that of the study of Ortiz et al. (2013). Such a discrepancy might be explained by imbalanced sample data in that study, where over 90% of the observations were not affected by outbreaks. By contrast, in our study, only 66% of the samples were taken from unaffected areas.

Compared to studies using a combination of C- and L-band co-polarized wavelengths (Ranson et al., 2003), this study showed that it is possible to delineate insect outbreaks using the cross-polarized channel, as relatively low commission errors were observed for the "affected" class. The relatively high commission errors for unaffected areas (about 30%) were related to the false classification of many affected pixels. Such errors result from low changes in the post-event SAR signal and might be related to an interplay between SAR acquisition timing, bark beetle phenology, and forest biomass levels. It is possible that infested trees had a relatively high trunk water content at SAR acquisition and that high biomass levels compensated for the decreased SAR signal caused by drying foliage and branches. In such a scenario, the post-event SAR signal does not sufficiently decrease to allow the detection of outbreaks. As for windthrows, the use of more advanced classification methods based on support vector machines improved the results only marginally, with the overall accuracies increasing by about 1%.

Areas susceptible to insect outbreaks might be detected with one-year lead time, but also with increased commission errors (55%). Early detection, as compared to optic sensors, might be related to tree stages after infestation (green, red, gray). SAR data are sensitive to vegetation water content, which changes during the green stage. However, trees must reach the red or gray stages to be easily detected in the optical datasets. Early detection might become important for forest management by delineating areas likely to be affected by outbreaks, which would allow closer monitoring and longer lead times for tree clearing. Such early detection could not be confirmed for all post- to pre-event image combinations, which might be related to the generally low dynamic range observed for some post- to pre-event ratios and the use of mean seasonal values for the post-event datasets used to calculate the ratios. As indicated above, the use of mean values has the potential to reduce signal variations owing to background environmental conditions. However, given that only few images were available for each year and the environmental conditions at acquisition varied markedly, the resulting sRCR values had a reduced dynamic range.

6. Conclusions

This study assessed L-band sensitivity to windthrows and insect-related forests disturbances and demonstrated the potential of space-borne L-band backscatter to identify such areas within a change-detection framework. The results suggest that disturbance events can be delineated using relatively simple thresholding approaches. An important outcome of this study was the demonstration of the potential to identify areas vulnerable to insect outbreaks, which might provide a distinct advantage (early warning) over the use of other sensor types. The methods presented here can be currently applied using L-band data from the ALOS-2 PALSAR-2 and from future L-band missions, such NASA-ISRO SAR.

The classification accuracy for the areas by affected windthrows was high, but lower when the disturbance was caused by insect outbreaks. A differentiated result was not unexpected because backscatter changes are more abrupt for windthrows (days) than for insect outbreaks (months or years). Overall, it seems that changes in backscatter owing to insect outbreaks or windthrows are too generic to identify the specific stressor. As other agents (e.g., fire, logging) could result in similar backscatter change values, a differential diagnosis using SAR remote-sensing data alone is limited. Therefore, ancillary information might be needed to pinpoint the exact disturbance agent, as shown in other studies.

Overall, the analysis proved to be complex because of the multitude of factors affecting backscatter changes (bark beetle outbreaks, logging, environmental conditions affecting the vegetation water content, and soil surface moisture) and limitations due to the density of SAR observations. Changes in the SAR backscatter were related to bark beetle outbreaks, with lower mean values of affected areas than of undisturbed forests. However, backscatter variations caused by other factors affected RCR values and might obscure effect of outbreaks if not properly filtered out. Indeed, for images acquired under heavy rainfall and freezing temperatures, the ability of RCR to differentiate affected areas was reduced; the observed dynamic range was low and most pixel values showed no change. Furthermore, changes from wet to dry periods could result in a decreased backscatter marked as insect-related disturbance even though it is only related to vegetation hydric stress. Therefore, a more detailed analysis using denser time series acquired during insect outbreak is needed to understand the influence of changing environmental factors.

Acknowledgments

This study was carried out within the framework of ECOPOTENTIAL, a European-funded H2020 project (grant No. 641762). ALOS PALSAR data were provided by the Japanese Space Agency (JAXA) within the 4th ALOS Research Announcement (PI 1091). We thank Karen Brune for language revision.

References

Bashfield, A., Keim, A., 2011. Continent-wide DEM Creation for the European Union. In: 34th International Symposium on Remote Sensing of Environment. The GEOSS Era: Towards Operational Environmental Monitoring. Sydney, Australia 10–15 April 2011. ISPRS.

Cailleret, M., Heurich, M., Bugmann, H., 2014. Reduction in browsing intensity may not compensate climate change effects on tree species composition in the Bavarian Forest National Park. For. Ecol. Manag. 328, 179–192.

Cartus, O., Santoro, M., Kellndorfer, J., 2012. Mapping forest aboveground biomass in the northeastern United States with ALOS PALSAR dual-polarization L-band. Remote Sens. Environ. 124, 466–478.

Cohen, W., Yang, Z., Kennedy, R., 2010. Detecting trends in forest disturbance and recovering using yearly Landsat time-series: 2. TimeSync-Tools for calibration and validation. Remote Sens. Environ. 114, 2911–2924.

Dale, V.H., Joyce, L.A., McNulty, S., Neilson, R.P., Ayres, M.P., Flannigan, M.D., Hanson, P.J., Irland, L.C., Lugo, A.E., Peterson, C.J., Simberloff, D., Swanson, F.J., Stocks, B.J., Wotton, M., 2001. Climate change and forest disturbances. Biogeosceinces 51, 723–734.

Eriksson, L.E.B., Fransson, J.E.S., Soja, M.J., Santoro, M., 2012. Backscatter signatures of wind-thrown forest in satellite SAR images. In: International Geoscience and Remote Sensing Symposium (IGARSS), pp. 6435–6438.

Fahse, L., Heurich, M., 2011. Simulation and analysis of outbreaks of bark beetle infestations and their management at the stand level. Ecol. Model. 222, 1833–1846.

Fassnacht, F.E., Latifi, H., Ghosh, A., Joshi, P.K., Koch, B., 2014. Assessing the potential of hyperspectral imagery to map bark beetle-induced tree mortality. Remote Sens. Environ. 140, 533–548.

Franklin, J.F., Spies, T.A., van Pelt, R., Carey, A.B., Thornburgh, D.A., Berg, D.R., Lindenmayerf, D.B., Harmong, M.E., Keetona, W.S., Shawh, D.C., Biblea, K., Chen, J., 2002. Disturbances and structural development of natural forest ecosystems with silvicultural implications, using Douglas fir forests as an example. For. Ecol. Manag. 155, 399–423.

Fransson, J.E.S., Walter, F., Gustavsson, A., Ulander, L.M.H., 2002. Detection of storm-damaged forested areas using airborne CARABAS-II VHF SAR image data. IEEE Trans. Geosci. Remote Sens. 40, 2170–2175.

Fransson, J.E.S., Pantze, A., Eriksson, L.E.B., Soja, M.J., Santoro, M., 2010. Mapping of wind-thrown forests using satellite SAR images. In: International Geoscience and Remote Sensing Symposium (IGARSS), pp. 1242–1245.

Frey, O., Santoro, M., Werner, C.L., Wegmüller, U., 2013. DEM-based SAR pixel-area estimation for enhanced geocoding refinement and radiometric normalization. Geosci. Remote. Sens. Lett. IEEE 10, 48–52.

Frolking, S., Palace, M.W., Clark, D.B., Chambers, J.Q., Shugart, H.H., Hurtt, G.C., 2009. Forest disturbance and recovery: a general review in the context of spaceborne remote sensing of impacts on aboveground biomass and canopy structure. J. Geophys. Res. Biogeosci. 114 (G2).

Green, R.M., 1998. The sensitivity of SAR backscatter to forest windthrow gaps. Int. J. Remote Sens. 19, 2419–2425.

Heurich, M., Beudert, B., Rall, H., Krenova, Z., 2010a. National parks as model regions for interdisciplinary long-term ecological research. M.e. al. (Ed.) In: Long-term Ecological Research. Between Theory and Application. Springer, Netherland, pp. 327–344.

Heurich, M., Ochs, T., Andresen, T., Schneider, T., 2010b. Object-orientated image analysis for the semi-automatic detection of dead trees following a spruce bark beetle (*Ips typographus*) outbreak. Eur. J. For. Res. 129, 313–324.

Huang, C., Goward, S.N., Masek, J.G., Thomas, N., Zhu, Z., Vogelmann, J.E., 2010. An automated approach for reconstructing recent forest disturbance history using dense Landsat time series stacks. Remote Sens. Environ. 114, 183–198.

Joshi, N., Mitchard, E.T., Woo, N., Torres, J., Moll-Rocek, J., Ehammer, A., Collins, M., Jepsen, M.R., Fensholt, R., 2015. Mapping dynamics of deforestation and forest degradation in tropical forests using radar satellite data. Environ. Res. Lett. 10, 34014.

Kalogirou, V., Ferrazzoli, P., Vecchia, A.D., Foumelis, M., 2014. On the SAR backscatter of burned forests: a model-based study in C-band, over burned pine canopies. IEEE Trans. Geosci. Remote Sens. 52, 6205–6215.

Kennedy, R.E., Yang, Z., Cohen, W.B., 2010. Detecting trends in forest disturbance and recovery using yearly Landsat time series: 1. LandTrendr — temporal segmentation algorithms. Remote Sens. Environ. 114, 2897–2910.

Kuntz, S., Siegert, F., 1999. Monitoring of deforestation and land use in Indonesia with multitemporal ERS data. Int. J. Remote Sens. 20, 2835–2853.

Kurz, W.A., Dymond, C.C., Stinson, G., Rampley, G.J., Neilson, E.T., Carroll, A.L., Ebata, T., Safranyik, L., 2008. Mountain pine beetle and forest carbon feedback to climate change. Nature 452, 987–990.

Lausch, A., Fahse, L., Heurich, M., 2010. Factors of the spatial-temporal dispersion of bark beetle in the Bavarian Forest National Park from 1990 to 2007 – a quantitative landscape-level-analysis. For. Ecol. Manag. 261, 233–245.

Lausch, A., Heurich, M., Gordalla, D., Dobner, H.J., Gwillym-Margianto, S., Salbach, C., 2013. Forecasting potential bark beetle outbreaks based on spruce forest vitality using hyperspectral remote-sensing techniques at different scales. For. Ecol. Manag. 308, 76–89.

Le Toan, T., Beaudoin, A., Guyon, D., 1992. Relating forest biomass to SAR data. IEEE Trans. Geosci. Remote Sens. 30, 403–411.

Lierop, P.v., Lindquist, E., Sathyapala, S., Franceschini, G., 2015. Global forest area disturbance from fire, insect pests, diseases and severe weather events. For. Ecol. Manag. 352, 78–88.

Lucas, R., Armston, J., Fairfax, R., Fensham, R., Accad, A., Carreiras, J., Kelley, J., Bunting, P., Clewley, D., Bray, S., Metcalfe, D., Dwyer, J., Bowen, M., Eyre, T., Laidlaw, M., Shimada, M., 2010. An evaluation of the ALOS PALSAR L-band backscatter - above ground biomass relationship Queensland, Australia: impacts of surface moisture condition and vegetation structure. IEEE J. Sel. Top. Appl. Earth Obs. Remote Sens. 3, 576–593.

Marini, L., Økland, B., Jönsson, A.M., Bentz, B., Carroll, A., Forster, B., Grégoire, J.-C., Hurling, R., Nageleisen, L.M., Netherer, S., Ravn, Hans Peter, Weed, A., Schroeder, M., 2017. Climate drivers of bark beetle outbreak dynamics in Norway spruce forests. Ecography 40, 1–10.

Mermoz, S., Le Toan, T., 2016. Forest disturbances and regrowth assessment using ALOS PALSAR data from 2007 to 2010 in Vietnam, Cambodia and Lao PDR. Remote Sens. 8, 2072–4292.

Mitchard, E.T.A., Saatchi, S.S., Lewis, S.L., Feldpausch, T.R., Woodhouse, I.H., Sonké, B., Rowland, C., Meir, P., 2011. Measuring biomass changes due to woody encroachment and deforestation/degradation in a forest–savanna boundary region of central Africa using multi-temporal L-band radar backscatter. Remote Sens. Environ. 115, 2861–2873.

Nielsen, M.M., Heurich, M., Malmberg, B., Brun, A., 2014. Automatic mapping of standing dead trees after an insect outbreak using the window independent context segmentation method. J. For. 112, 564–571.

Oeser, J., Pflugmacher, D., Senf, C., Heurich, M., Hostert, P., 2017. Using intra-annual Landsat time series for attributing forest disturbance agents in Central Europe.

Forest 8.
Olofsson, P., Foody, G.M., Herold, M., Stehman, S.V., Woodcock, C.E., Wulder, M.A., 2014. Good practices for estimating area and assessing accuracy of land change. Remote Sens. Environ. 148, 42–57.
Ortiz, S.M., Breidenbach, J., Kändler, G., 2013. Early detection of bark beetle green attack using TerraSAR-X and RapidEye data. Remote Sens. 5, 1912–1931.
Polewski, P., Yao, W., Heurich, M., Krzystek, P., Stilla, U., 2015. Detection of single standing dead trees from aerial color infrared imagery by segmentation with shape and intensity priors. ISPRS Ann. Photogramm. Remote. Sens. Spat. Inf. Sci. 2 (3), 181–188.
Quegan, S., Toan, T.L., Yu, J.J., Ribbes, F., Floury, N., 2000. Multitemporal ERS SAR analysis applied to forest mapping. IEEE Trans. Geosci. Remote Sens. 38, 741–752.
Ranson, K.J., Kovacs, K., Sun, G., Kharuk, V.I., 2003. Disturbance recognition in the boreal forest using radar and Landsat-7. Can. J. Remote. Sens. 29, 271–285.
Rignot, E.J.M., Zyl, J.J.v., 1993. Change detection techniques for ERS-1 SAR data. IEEE Trans. Geosci. Remote Sens. 31, 896–906.
Santoro, M., Askne, J., Smith, G., Fransson, J.E.S., 2002. Stem volume retrieval in boreal forests from ERS-1/2 interferometry. Remote Sens. Environ. 81, 19–35.
Santoro, M., Pantze, A., Fransson, J.E.S., Dahlgren, J., Persson, A., 2012. Nation-wide clear-cut mapping in Sweden using ALOS PALSAR strip images. Remote Sens. 4, 1693–1715.
Schlyter, P., Stjernquist, I., Bärring, L., Jönsson, A.M., Nilsson, C., 2006. Assessment of the impacts of climate change and weather extremes on boreal forests in northern Europe, focusing on Norway spruce. Clim. Res. 31, 75–84.
Schwarz, M., Steinmeier, C., Holecz, F., Stebler, O., Wagner, H., 2003. Detection of windthrow in mountainous regions with different remote sensing data and classification methods. Scand. J. For. Res. 18, 525–536.
Seidl, R., Schelhaas, M.J., Rammer, W., Verkerk, P.J., 2014. Increasing forest disturbances in Europe and their impact on carbon storage. Nat. Clim. Chang. 4, 806–810.
Seidl, R., Müller, M., Hothorn, T., Bässler, C., Heurich, M., Kautz, M., 2016. Small beetle, large-scale drivers: how regional and landscape factors affect outbreaks of the European spruce bark beetle. J. Appl. Ecol. 53, 530–540.
Senf, C., Seidl, R., Hostert, P., 2017. Remote sensing of forest insect disturbances: current state and future directions. International Journal of Applied Earth Observation and Geoinformation. (in press).
Shimada, M., Isoguchi, O., Tadono, T., Isono, K., 2009. PALSAR radiometric and geometric calibration. IEEE Trans. Geosci. Remote Sens. 47, 3915–3932.
Shimada, M., Itoh, T., Motooka, T., Watanabe, M., Shiraishi, T., Thapa, R., Lucas, R., 2014. New global forest/non-forest maps from ALOS PALSAR data (2007–2010). Remote Sens. Environ. 155, 13–31.
Tanase, M.A., de la Riva, J., Santoro, M., Le Toan, T., Perez-Cabello, F., 2010. Sensitivity of X-, C- and L-band SAR backscatter to fire severity in Mediterranean pine forests. IEEE Trans. Geosci. Remote Sens. 48, 3663–3675.
Tanase, M.A., Panciera, R., Lowell, K., Tian, S., Garcia-Martin, A., Walker, J.P., 2014. Sensitivity of L-band radar backscatter to forest biomass in semi-arid environments: a comparative analysis of parametric and non-parametric models. IEEE Trans. Geosci. Remote Sens. 52, 1–15.
Tanase, M., Ismail, I., Lowell, K., Karyanto, O., Santoro, M., 2015a. Detecting and quantifying forest change: the potential of existing C- and X-band radar datase. PLoS ONE 10 (6), e0131079 (1–14).
Tanase, M.A., Kennedy, R., Aponte, C., 2015b. Radar burn ratio for fire severity estimation at canopy level: an example for temperate forests. Remote Sens. Environ. 170, 14–31.
Thiel, C.J., Thiel, C., Schmullius, C.C., 2009. Operational large-area forest monitoring in Siberia using ALOS PALSAR summer intensities and winter coherence. IEEE Trans. Geosci. Remote Sens. 47, 3993–4000.
Turner, M.G., Baker, W.L., Peterson, C.J., Peet, R.K., 1998. Factors influencing succession: lessons from large, infrequent natural disturbances. Ecosystems 1, 511–523.
Weed, A.S., Ayres, M.P., Hicke, J.A., 2013. Consequences of climate change for biotic disturbances in North American forests. Ecol. Monogr. 83, 441–470.
Wegmüller, U., Werner, C., Strozzi, T., Wiesmann, A., 2002. Automated and precise image registration procedures. In: Bruzzone, L., Smits, P. (Eds.), Analysis of Multi-temporal Remote Sensing Images. World Scientific, Singapore, pp. 37–49 (2002).
Wermelinger, B., 2004a. Ecology and management of the spruce bark beetle *Ips typographus*—a review of recent research. For. Ecol. Manag. 202, 67–82.
Wermelinger, B., 2004b. Ecology and management of the spruce bark beetle *Ips typographus* - a review of recent research. For. Ecol. Manag. 202, 67–82.
Werner, C., Wegmuller, U., Strozzi, T., Wiesmann, A., 2005. Precision estimation of local offsets between pairs of SAR SLCs and detected SAR images. In: Geoscience and Remote Sensing Symposium. IEEE, Seoul, pp. 4803–4805.
Westerling, A.L., Hidalgo, H.G., Cayan, D.R., Swetnam, T.W., 2006. Warming and earlier spring increase western US forest wildfire activity. Science 313 (5789), 940–943.
Wulder, M.A., Dymond, C.C., White, J.C., Leckie, D.G., Carroll, A.L., 2006. Surveying mountain pine beetle damage of forests: a review of remote sensing opportunities. For. Ecol. Manag. 221, 27–41.
Zeppenfeld, T., Svoboda, M., DeRose, R.J., Heurich, M., Müller, J., Čížková, P., Starý, M., Bače, R., Donato, D.C., 2015. Response of mountain *Picea abies* forests to stand-replacing bark beetle outbreaks: neighbourhood effects lead to self-replacement. J. Appl. Ecol. 52, 1402–1411.